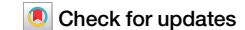
Published in partnership with CECCR at King Abdulaziz University



https://doi.org/10.1038/s41612-025-01050-8

Assimilating summer sea ice thickness enhances predictions of Arctic sea ice and surrounding atmosphere within two months



Anling Liu¹, Jing Yang¹⊠, Qing Bao², Frederic Vitart³, Jiping Liu⁴, Xi Liang⁵, Mengqian Lu^{6,7}, Seong-Joong Kim³, Daoyi Gong¹, Zhongxiang Tian⁵ & Hongbo Liu²

Subseasonal prediction of Arctic sea ice and associated atmospheric conditions during the melting season remains challenging due to limited understanding of sea ice initial conditions. This study integrates sea ice assimilation into the coupled model FGOALS-f2 using the localized error subspace transform ensemble Kalman filter, and conducts subseasonal predictions starting from August 1st over 2004–2023. Results show that simultaneous assimilation of sea ice concentration (SIC) and thickness (SIT) significantly improves sea ice predictions for up to two months, while assimilating SIC alone primarily benefits one-month lead predictions. SIT assimilation provides added predictive value for surface air temperature (SAT) forecasts beyond SIC assimilation alone, effectively extending the atmospheric influence of sea ice initial conditions to two months. This improvement in SAT predictions is primarily attributed to a more realistic representation of the surface energy budget. These findings highlight the pivotal role of summer SIT assimilation to enhance subseasonal predictions in the Arctic and challenge the conventional view that initial conditions affect only short-term forecasts. This study underscores the necessity for better representation of ice–atmosphere interactions in models and advocates for enhanced observational capabilities for summer SIT to improve subseasonal predictions in the Arctic and surrounding regions.

The Arctic region plays a pivotal role in the global climate system, with its sea ice cover serving as a crucial modulator of energy exchanges between the atmosphere and ocean^{1,2}. Accurate subseasonal prediction of Arctic sea ice and its associated atmospheric conditions, particularly during August and September when sea ice reaches its peak melting and annual minimum, is essential for scientific research^{3,4}, marine navigation^{5–7}, and environmental management^{8–10}. However, precise subseasonal predictions (typically ranging from two weeks to two months) during this period remain challenging for current dynamical operational systems¹¹. The intricate interactions among sea ice, ocean,

and atmosphere complicate forecasting efforts^{11–13}, often leading to a rapid decline in prediction skill beyond a few weeks^{14,15}.

A primary limitation in current dynamical models for subseasonal prediction of Arctic sea ice is the insufficient understanding of the role of sea ice initial conditions^{3,16,17}. While sea ice concentration (SIC) is routinely assimilated into models and has been shown to improve short-term predictions of SIC^{17–19}, its effect tends to diminish quickly over longer lead times, especially during the melting season^{20,21}. The dynamic changes during the melting season make it difficult for SIC assimilation alone to sustain accurate predictions of ice evolution, particularly in the marginal ice

¹State Key Laboratory of Earth Surface Processes and Hazards Risk Governance (ESPHR), Faculty of Geographical Science, Beijing Normal University, Beijing, China. ²State Key Laboratory of Numerical Modeling for Atmospheric Sciences and Geophysical Fluid Dynamics (LASG), Institute of Atmospheric Physics, Chinese Academy of Sciences, Beijing, China. ³European Centre for Medium-Range Weather Forecasts (ECMWF), Reading, UK. ⁴School of Atmospheric Sciences, Sun Yat-sen University, Zhuhai, China. ⁵Key Laboratory of Marine Hazards Forecasting, National Marine Environmental Forecasting Center, Ministry of Natural Resources, Beijing, China. ⁵Department of Civil and Environmental Engineering, The Hong Kong University of Science and Technology, Hong Kong SAR, China. ⁵Coto Poon Centre for Climate Resilience and Sustainability, The Hong Kong University of Science and Technology, Hong Kong SAR, China. ⁵Korea Polar Research Institute, Incheon, South Korea. ⊠e-mail: yangjing@bnu.edu.cn

zones^{22,23}. In contrast, sea ice thickness (SIT) has been demonstrated to possess longer memory than SIC in numerical simulations, rendering it a potential predictor for longer lead times^{24–27}. Previous studies have shown that assimilating satellite-retrieved SIT observations during winter and spring can enhance subseasonal-to-seasonal predictions of SIC^{22,21} However, recent research has identified a spring predictability barrier in Arctic sea ice—a specific date in spring after which predictions can reliably forecast summer sea ice, while predictions initialized before this date exhibit significantly lower skill^{31–33}. In light of this barrier, it is crucial to investigate the potential impact of assimilating summer SIT on sea ice predictions. But this area remains underexplored due to the challenges in acquiring summer SIT observations. Landy et al. (2022) address this by combining deep learning with numerical simulations of the Cryosat-2 radar altimetry response to generate the first year-round Arctic SIT observations³⁴. The latest studies have shown that assimilating this dataset during summer can improve September sea ice predictions^{35,36}. Nevertheless, the limited temporal coverage of these observations underscores the need for multi-year reforecasts to gain a more comprehensive understanding of the impact of summer SIT assimilation on subseasonal sea ice prediction.

One challenge in subseasonal atmospheric prediction is the unclear role of initial and boundary conditions at such a timescale^{37–40}. While the impact of atmospheric initial conditions on short-term weather forecasts is well identified, the limited memory of the atmosphere makes it difficult to influence subseasonal prediction^{37,41,42}. Therefore, it is essential to explore potential sources of subseasonal predictability from components with longer memory to improve and understand subseasonal predictions. Sea ice has been reported to exhibit long memory and can influence local and distant atmospheric variations after several weeks to months, as demonstrated by observational data and numerical simulations^{43–46}. Additionally, some studies using atmospheric models have shown that initial perturbations in SIC can improve extended-range forecasts for mid-to-high latitudes^{47–49}. However, it remains unclear to what extent and for how long the sea ice initial conditions can affect the subseasonal atmospheric prediction within a fully coupled dynamical prediction system.

By conducting multi-year re-forecasts initialized on August 1st, this study aims to: (1) identify the impact of sea ice assimilation, particularly summer SIT, on subseasonal Arctic sea ice and atmospheric predictions during August and September, and (2) investigate the mechanisms through which sea ice initialization influences atmospheric predictability on subseasonal timescales using a fully coupled dynamical model. We seek to deepen the understanding of sea ice–atmosphere interactions on subseasonal timescales and provide insights for improving operational predictions.

Results

Improved sea ice initial conditions through optimized initialization

Accurate subseasonal prediction of sea ice and associated atmospheric conditions during August and September is essential but remains challenging in current operational systems, as mentioned in the introduction. As shown in Fig. 1, the FGOALS-f2 system^{50,51}, which does not incorporate sea ice assimilation (hereafter referred to as the Control experiment), exhibits errors in both the SIC initial conditions of early August and the subsequent one-to-two-month SIC predictions during the hindcast period from 2004 to 2023. We first calculate the mean absolute error (MAE; see Methods for details) to assess the prediction skill of SIC spatial distribution. The MAE of initial SIC on August 1st is 0.11, corresponding to 25% of the weighted mean observed SIC. The initial SIC in the Control experiment is overestimated by more than 15% over the northern Barents-Kara Seas and East Greenland Sea, while underestimated by 5-40% over the Central Arctic Ocean, East Siberian Sea, and northern Laptev Sea (Fig. 1g). In the one-month lead prediction for August, the MAE increases by 18%, ranging from 0.11 to 0.13, mainly due to further underestimation of SIC in the Central Arctic Ocean (Fig. 1h). In September, most regions are underestimated by more than 30%, causing the MAE to rise further by 31%, from 0.13 to 0.17 (Fig. 1i). The initial biases are amplified in the subseasonal prediction. Therefore, we will

identify the optimum sea ice parameters for initialization and investigate whether and how optimizing sea ice initialization can improve the one-to-two-month lead predictions.

SIC and SIT are pivotal parameters for characterizing the state and dynamics of sea ice. Utilizing a localized error subspace transform ensemble Kalman filter (LESTKF, see Methods for details)⁵² provided by the Parallel Data Assimilation Framework (PDAF)⁵³, we carry out two sets of re-forecasts: one with SIC assimilation alone (hereafter referred to as the SIC-only experiment), and the other with simultaneous assimilation of both SIC and SIT (hereafter referred to as the SIC-SIT experiment). The assimilation experiments start on August 1st, producing predictions for the next two months of each year during the hindcast period 2004–2023.

The SIC-only experiment shows substantial improvements in the initial SIC relative to the Control experiment. The MAE of initial SIC significantly decreases by 55%, from 0.11 to 0.05. Overestimations in the northern Barents-Kara Seas and East Greenland Sea, as well as underestimations over the Central Arctic Ocean, East Siberian Sea, and Laptev Sea, are reduced to less than 15% in most regions (Fig. 2c). In the SIC-SIT experiment, the initial SIC further improves compared to the SIC-only experiment, with the MAE decreasing by 20%, from 0.05 to 0.04 (Fig. 2d). The improvements mainly occur in the marginal ice zones, particularly in the northern Barents-Kara Seas and East Siberian Sea.

In addition to the SIC improvements, the initial SIT is also significantly improved in the SIC-SIT experiment compared to the Control and SIC-only experiments (Fig. 3). In the Control experiment, SIT is overestimated in the marginal ice zones (including the northern Barents-Kara Seas, East Greenland Sea, and the Canadian Archipelago) and underestimated in the Central Arctic Ocean (Fig. 3e). In most regions, SIT errors exceed 0.4 meters, suggesting a relatively large bias in the model. While SIC assimilation improves the initial SIC, it does not explicitly correct these SIT errors, leaving the SIT biases largely unchanged (Fig. 3f). In contrast, the SIC-SIT experiment effectively reduces the SIT biases across the Arctic (Fig. 3g). The reduction of initial SIT biases leads to a more realistic sea ice state, which likely enhances the consistency between SIC and SIT.

To further quantify the improvements in sea ice initialization, we employ the Brier Score (BS)⁵⁴ to evaluate the ability to capture the ice edge position and occurrence probability (Fig. 4). Lower BS scores indicate higher skill, reflecting that the initial conditions of the model ensembles are more consistent with the observations, as detailed in the Methods. In the Control experiment, the initial SIC exhibits relatively low consistency with observations, with a 20-year averaged BS score of 0.091. The SIC-only experiment enhances the skill of initial SIC by 40%, reducing the BS score from 0.091 to 0.055. In the SIC-SIT experiment, the skill of the initial SIC is further improved, though only marginally compared to the SIC-only experiment, with a reduction in BS from 0.055 to 0.049.

These results indicate that sea ice assimilation significantly enhances the accuracy of sea ice initial conditions. The simultaneous assimilation of both SIC and SIT produces more realistic initial conditions than SIC assimilation alone, suggesting that this combined approach could be the optimal strategy for sea ice initialization.

Optimizing initialization for enhanced subseasonal sea ice prediction

Having demonstrated the improvements in the initial conditions through sea ice assimilation, the next step is to assess how these enhancements impact the subsequent one-to-two-month sea ice predictions. To address this, we evaluate the prediction skill for August and September based on the two initialization strategies mentioned above: the SIC-only and SIC-SIT experiments.

Compared to the Control experiment, the SIC-only experiment shows a marked improvement in the prediction skill of monthly mean SIC distribution for August. The MAE of August mean SIC decreases by 23%, from 0.13 to 0.10 (Fig. 5e). The most notable improvements occur over the northern Barents-Kara Seas, Central Arctic Ocean, East

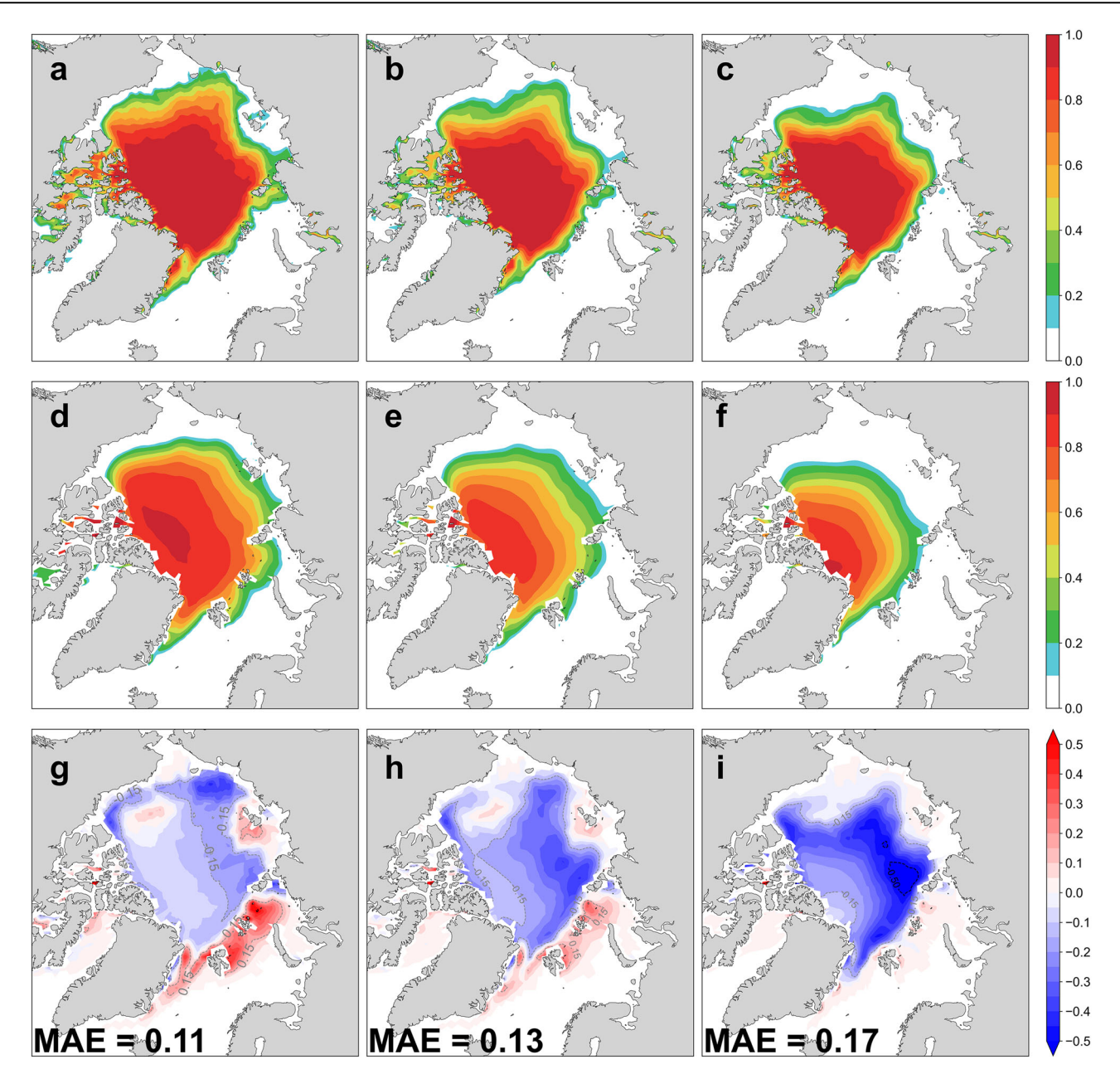


Fig. 1 | Observed and Control experiment (without sea ice assimilation) sea ice concentration (SIC) and their differences in the Arctic (2004–2023 average). The spatial distribution of observed mean SIC on (a) August 1st, (b) August, (c) September. The spatial distribution of mean SIC from the Control experiment on (d) August 1st, (e) August, (f) September. The differences of mean SIC between the

Control experiments and observations on (g) August 1st, (h) August, (i) September. Only the differences that exceed the 95% confidence level using a two-tailed Student's t-test are presented, with the mean absolute error (MAE) indicated in the bottom left corner.

Siberian Sea, and northern Laptev Sea regions. Despite better SIC initial conditions, no noticeable enhancement is achieved in September. The MAE for the two-month lead prediction of SIC decreases only slightly, from 0.17 to 0.16 (Fig. 5f). The underestimation of SIC over the Central Arctic Ocean persists even with improved SIC initial conditions.

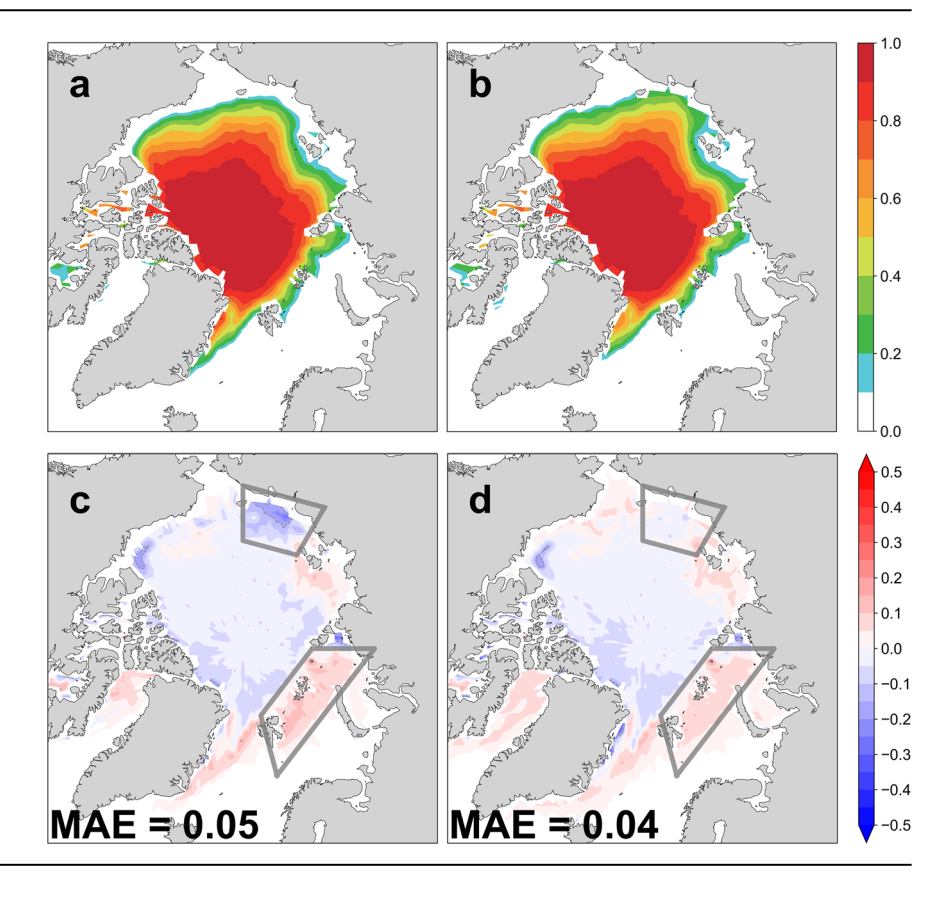
In the SIC-SIT experiment, the prediction skill of the mean SIC distribution for both August and September is evidently improved. For August, the prediction skill is further enhanced compared to the SIC-only experiment, with the MAE decreasing by 40%, from 0.10 to 0.06 (Fig. 5g). The most notable improvements occur over the northern Laptev Sea and East Siberian Sea. In September, the SIC-SIT experiment shows a substantial enhancement in the prediction skill of monthly mean SIC distribution, outperforming both the Control and SIC-only experiments (Fig. 5h). The MAE of September mean SIC decreases by 47% and 44%, from 0.17 and 0.16

to 0.09, respectively. This improvement is mainly reflected in reduced biases over the Central Arctic Ocean.

To assess the impact of sea ice assimilation on predicting the interannual anomalies of sea ice, we calculate the anomaly correlation coefficient (ACC) and root mean square error (RMSE) of monthly mean sea ice extent (SIE) anomalies for the hindcast period 2004–2023. The SIE is defined as the total area of grid boxes with at least 15% SIC. Since the long-term trend dominates the total variability, we remove the linear trend from the SIE anomalies to focus on the interannual fluctuations.

For the one-month lead prediction in August, the Control experiment shows relatively low skill, with an ACC of 0.46 and an RMSE of 0.45 (Fig. 6). The SIC-only experiment evidently enhances the prediction skill, increasing the ACC to 0.70 and reducing the RMSE to 0.32. The SIC-SIT experiment

Fig. 2 | Initial SIC on August 1st for different assimilation experiments and their differences from observations (2004–2023 average). The spatial distribution of mean SIC from (a) the SIC-only experiment (assimilating SIC alone), (b) the SIC-SIT experiment (assimilating both SIC and SIT). The mean SIC differences: (c) SIC-only experiment minus observations, (d) SIC-SIT experiment minus observations. Only the differences that exceed the 95% confidence level using a two-tailed Student's t-test are presented, with the MAE indicated in the bottom left corner.



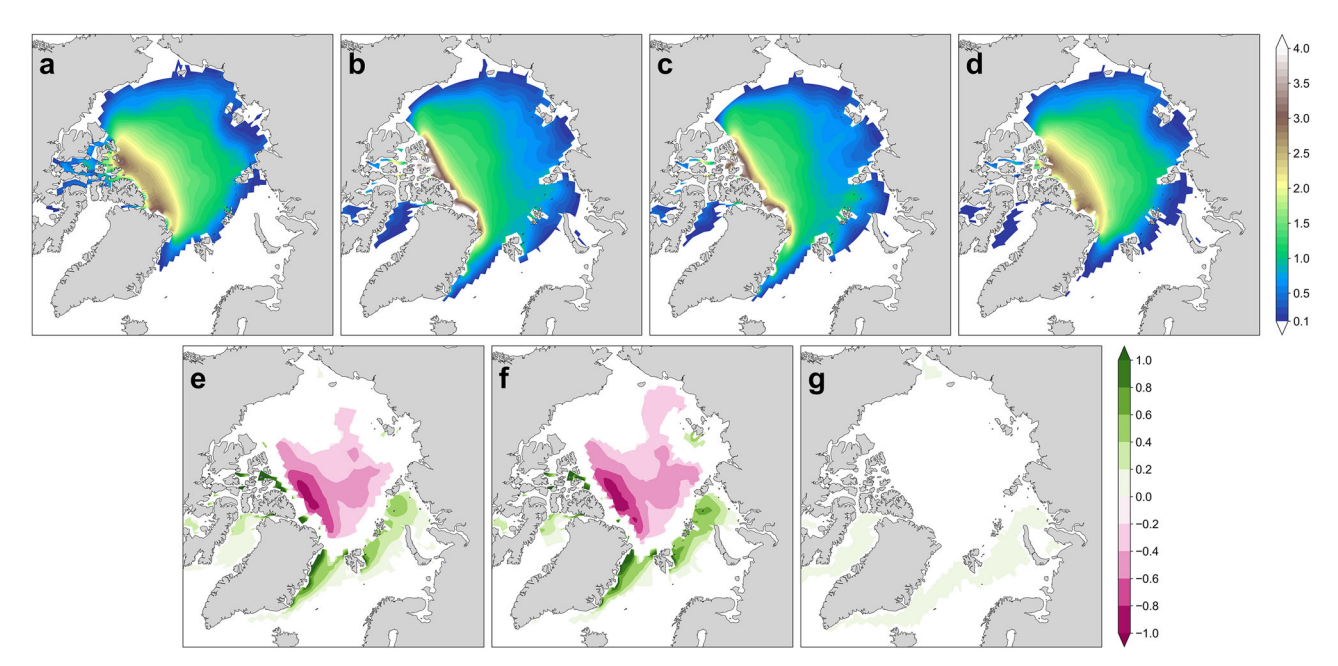


Fig. 3 | Initial SIT (m) on August 1st from Pan-Arctic Ice Ocean Modeling and Assimilation System (PIOMAS) and different experiments (2004–2023 average). The spatial distribution of mean SIT from (a) PIOMAS, (b) the Control experiment,

(c) the SIC-only experiment, and (d) the SIC-SIT experiment. The mean SIT differences: (e) Control experiment minus PIOMAS, (f) SIC-only experiment minus PIOMAS, and (g) SIC-SIT experiment minus PIOMAS.

achieves a greater improvement, with an ACC of 0.90 and an RMSE of 0.19, highlighting the added value of SIT assimilation.

The two-month lead prediction in September proves more challenging. In the Control experiment, the ACC decreases from 0.46 in August to 0.42 in September, accompanied by an increase in RMSE from 0.45 to 0.54. While the SIC-only experiment shows notable improvements in August, its skill drops sharply in September, with the

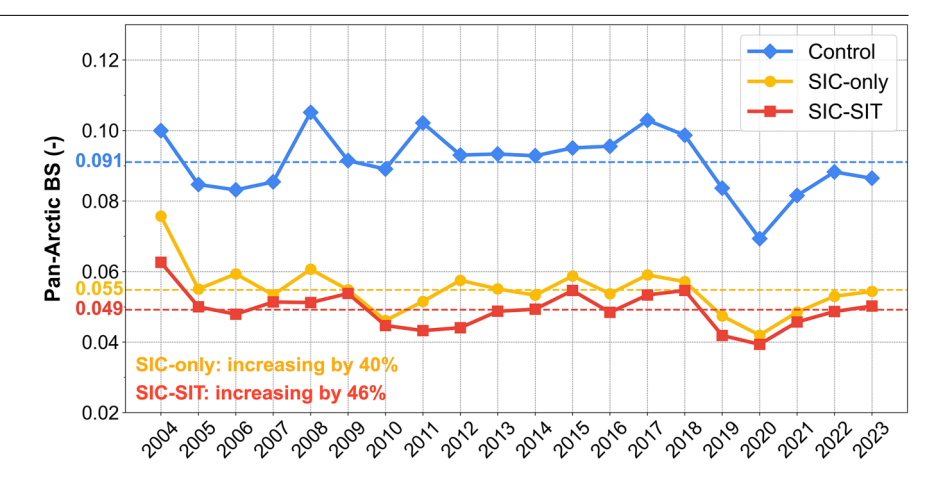
ACC falling from 0.70 to 0.49 and the RMSE rising from 0.32 to 0.49. This highlights the limitations of relying solely on SIC assimilation for longer lead-time predictions. Although the SIC-SIT experiment also experiences a decrease in prediction skill from August to September, it still demonstrates a substantial advantage over the other two experiments in September. The ACC reaches 0.82, representing a 95% improvement over the Control experiment and a 67% rise over the SIC-

only experiment. The RMSE reduces to 0.29, marking a substantial enhancement over both the Control and SIC-only experiments.

To examine whether the improvements from sea ice assimilation are consistent across different time scales, we also evaluate the weekly prediction

skill over the first eight weeks (Fig. S1). The MAE, ACC, and RMSE results consistently show that the SIC-only experiment improves prediction skill throughout the 8-week period compared to the Control experiment, with the most notable improvement occurring in the first two weeks. The

Fig. 4 | Yearly Pan-Arctic Brier Score (BS) for initial SIC on August 1st across different experiments (2004–2023). BS scores for initial SIC in the Control (blue line; average BS: 0.091), SIC-only (orange line; average BS: 0.055), and SIC-SIT (red line; average BS: 0.049) experiments. Dashed lines represent the 20-year averaged BS scores. The SIC-only and SIC-SIT experiments show a 40% and 46% increase in skill compared to the Control experiment, respectively.



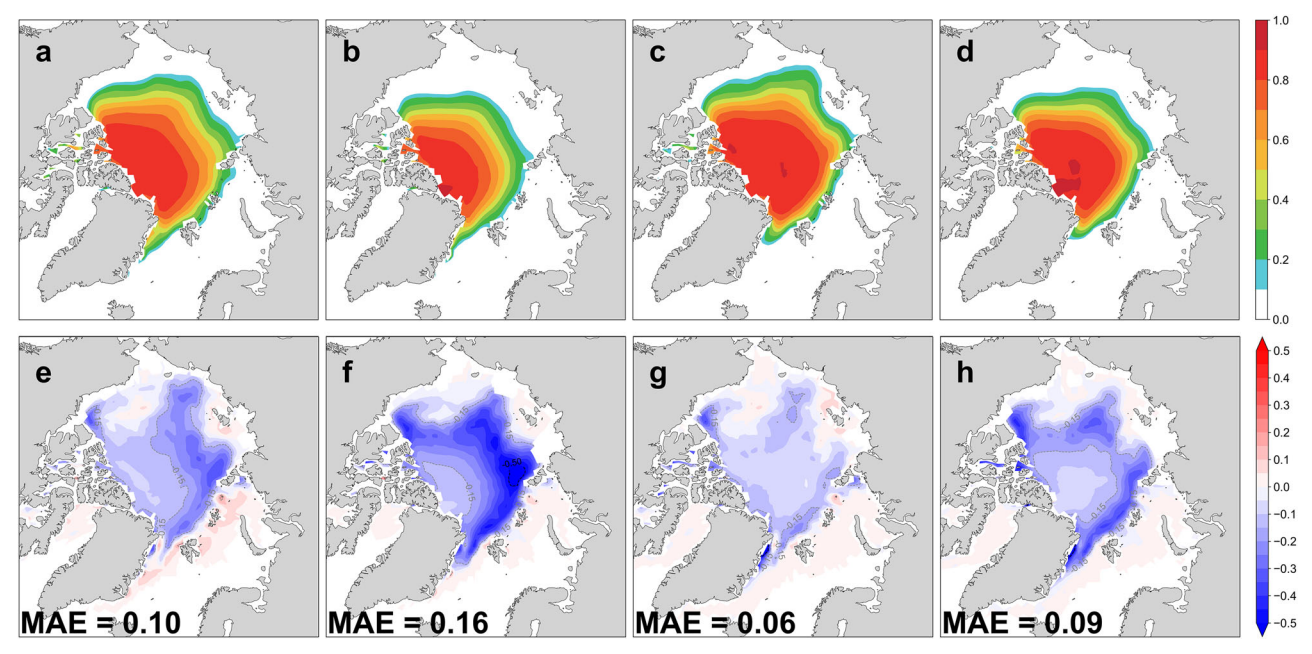
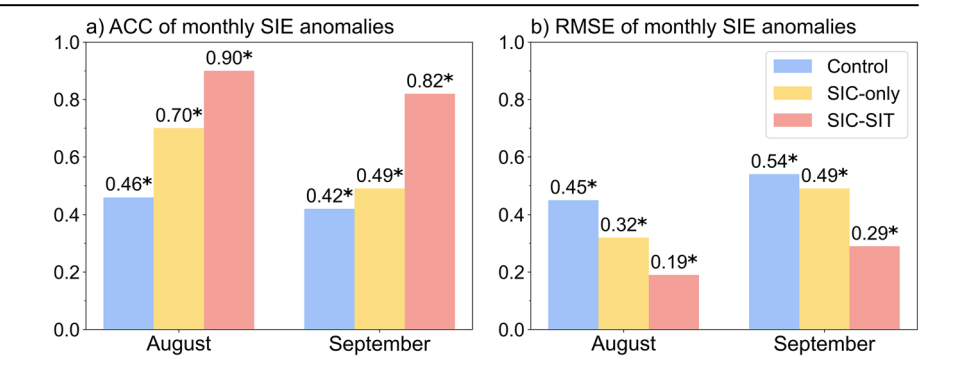


Fig. 5 | Arctic SIC in August and September for different assimilation experiments and their differences from observations (2004–2023 average). The spatial distribution of mean SIC from the SIC-only experiment in (a) August, (b) September, and from the SIC-SIT experiment in (c) August, (d) September. The mean

SIC differences: SIC-only experiment minus observations in (\mathbf{e}) August, (\mathbf{f}) September, and SIC-SIT experiment minus observations in (\mathbf{g}) August, (\mathbf{h}) September. Only the differences that exceed the 95% confidence level using a two-tailed Student's t-test are presented, with the MAE indicated in the bottom left corner.

Fig. 6 | Anomaly correlation coefficient (ACC) and Root Mean Square Error (RMSE) for monthly sea ice extent (SIE) anomalies in August and September (2004–2023). a ACC between observations and three prediction experiments: Control (blue bar), SIC-only (orange bar), and SIC-SIT (red bar). Higher ACC values indicate better prediction skills. The numbers above the bars represent the ACC values for each experiment, with asterisks indicating statistical significance at the 95% confidence level based on a Monte Carlo test. b As in a, but for the RMSE. Lower RMSE values indicate better prediction skills.



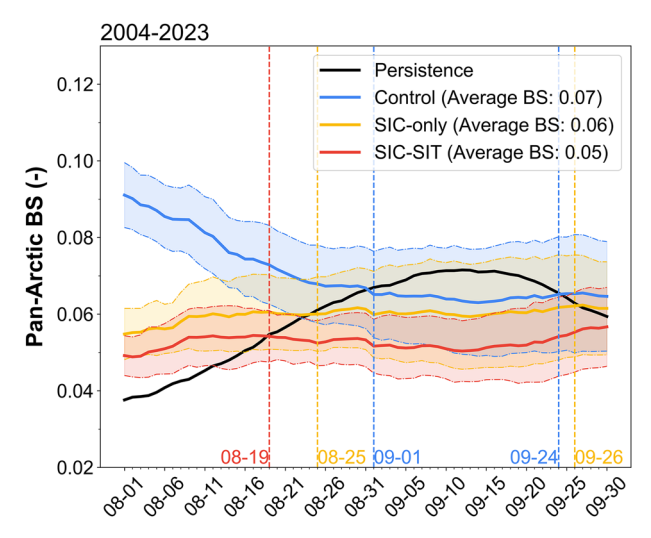


Fig. 7 | Pan-Arctic Brier Score (BS) for daily SIC predictions for the hindcast period 2004–2023. BS scores for the Control (blue line; average BS: 0.07), SIC-only (orange line; average BS: 0.06), SIC-SIT (red line; average BS: 0.05) experiments, and persistence (black line). Shaded areas represent one standard deviation for each experiment. Dashed vertical lines mark key dates: August 19th, August 25th, September 1st, September 24th, and September 26th.

advantage weakens after week 3. In contrast, the SIC-SIT experiment demonstrates consistently higher prediction skill throughout the 8-week period, maintaining a significant advantage over both the Control and SIC-only experiments, particularly at longer lead times (e.g., 4-8 weeks).

These findings emphasize the necessity of SIT assimilation for subseasonal prediction, especially for overcoming the challenges of predicting sea ice variability over longer lead times.

Previous studies have demonstrated that sea ice exhibits memory on subseasonal timescales, a phenomenon known as persistence²⁵. Persistence has become a common benchmark for measuring the prediction skill of SIC^{14,21,55}. Here, we calculate BS scores of daily SIC to further assess the prediction skill from three sets of experiments, using persistence as a benchmark.

As shown in Fig. 7, in the Control experiment, BS scores for dynamical forecasts in August are higher than those for persistence, implying lower prediction skill. It surpasses persistence on September 1st and maintains higher skill for four weeks until September 24th. The SIC-only experiment enhances the prediction skill over the next two months, reducing the average BS score from 0.07 to 0.06. Assimilating SIC alone extends the period during which prediction skill exceeds persistence to five weeks, from August 25th to September 26th. The SIC-SIT experiment leads to further improvements in prediction skill throughout August and September. The average BS score decreases from 0.06 to 0.05, reflecting a more substantial enhancement in prediction accuracy. Assimilating both SIC and SIT enables the prediction skill to exceed persistence earlier, around August 19th, and sustains this advantage for over six weeks, extending through the end of September.

Therefore, SIC assimilation alone significantly improves the initial SIC and one-month lead prediction for August, but its impact on longer lead-time predictions (here for September) remains limited. In contrast, simultaneous assimilation of SIC and SIT not only refines the sea ice initial state but also leads to substantial improvements in subseasonal sea ice prediction for both August and September. This improvement is notable for longer lead-time predictions in September, underscoring the indispensable role of SIT in improving sea ice prediction during the melting season.

Refined sea ice initial conditions enhance subseasonal SAT predictions

Given the strong ice-atmosphere interactions^{56,57}, the improved initial conditions and subseasonal sea ice predictions are expected to enhance the

prediction skill of surface air temperature (SAT) on subseasonal timescales. Here, we investigate how different sea ice assimilation strategies influence SAT forecasts by comparing the SIC-only and SIC-SIT experiments with the Control experiment, focusing on the core Arctic areas where the sea ice variations are evident during the melting season.

As shown in Fig. 8a, the SAT predictions in the Control experiment for August exhibit significant cold biases across the core Arctic areas, including the Barents-Kara Seas, East Greenland Sea, Laptev Sea, Central Arctic Ocean, and the Canadian Archipelago. In most of these regions, the biases range from 1 to 3°C, indicating substantial prediction errors. In the SIC-only experiment, the cold biases are slightly reduced, with reductions of less than 0.2°C in most regions (Fig. 8d). These improvements are not statistically significant at the 95% confidence level, suggesting that SIC assimilation alone provides limited improvement in correcting the systematic cold biases. In contrast, cold biases in the SIC-SIT experiment are significantly reduced over the core Arctic areas, particularly in the northern Barents-Kara Seas, East Greenland Sea, Central Arctic Ocean, and the Canadian Archipelago, with reductions of 0.2 to 1°C (Fig. 8e).

In contrast to the dominant cold biases over most Arctic areas in August, the predictions for September SAT display an evident warm bias in the central Arctic (Fig. 9a) while the areas over the Barents-Kara Seas, East Greenland Sea, Laptev Sea, and the Canadian Archipelago still remain substantial cold biases in the Control experiment. The warm biases emerge in the Central Arctic Ocean and the Beaufort Sea, reaching up to 1.5 °C. SIC assimilation alone leads to minor improvements. The warm biases over the Central Arctic Ocean are slightly reduced by up to 0.3 °C, and the cold biases over the East Greenland Sea and Barents-Kara Seas decrease by about 0.1 to 0.3 °C (Fig. 9d). With SIT assimilation included, the SAT predictions show considerable improvements (Fig. 9e). The warm biases in the Central Arctic Ocean are reduced by up to 1°C and cold biases in the East Greenland Sea and Canadian Archipelago are reduced by more than 1°C. These findings confirm that SIT assimilation provides added predictive value for SAT forecasts beyond SIC assimilation alone, highlighting the importance of SIT initialization for subseasonal atmospheric prediction.

Surface budget improvements explain enhanced SAT predictions

Based on the above analysis, the simultaneous assimilation of SIC and SIT represents the optimal strategy for improving SAT forecasts. To further investigate the underlying mechanisms behind the improved SAT prediction skill, we compare the differences in surface budgets between the SIC-SIT and Control experiments, as shown in Figs. 10-11. In August, the overestimated SIC over the marginal seas, covering the northern Barents-Kara Seas, East Greenland Sea, and the Canadian Archipelago, are evidently reduced in the SIC-SIT experiment compared to the Control experiment (Fig. 10a). Accordingly, the decreased sea ice in these areas corresponds to a declined shortwave reflection, which causes a significant increase in net downward shortwave radiation, thereby raising the surface temperature (Fig. 10b). As surface warming increases the temperature gradient between the ocean surface and the lower atmosphere, the upward sensible heat flux and surface longwave radiation are amplified, further warming the lower atmosphere (Fig. 10c, d). As a result, the original cold biases of SAT are reduced and the SAT prediction acquires improvement.

Over the central Arctic region, the SAT biases are also reduced in August, but the mechanism differs from that in the marginal seas. In the SIC-SIT experiment, the underestimation of SIC over the central Arctic is corrected. Surprisingly, despite the increased SIC, the upward latent heat flux is observed to intensify (Fig. 10e). This indicates that surface water evaporation is enhanced, likely due to the proliferation of melt ponds on the ice surface. Melt ponds, with their lower albedo compared to the surrounding sea ice, absorb more shortwave radiation. However, the low thermal conductivity of sea ice limits the transfer of absorbed energy from the melt ponds to the underlying ocean. As a result, the energy remains trapped at the surface, leading to rapid warming of the melt ponds and surrounding ice surface. This surface warming increases the surface

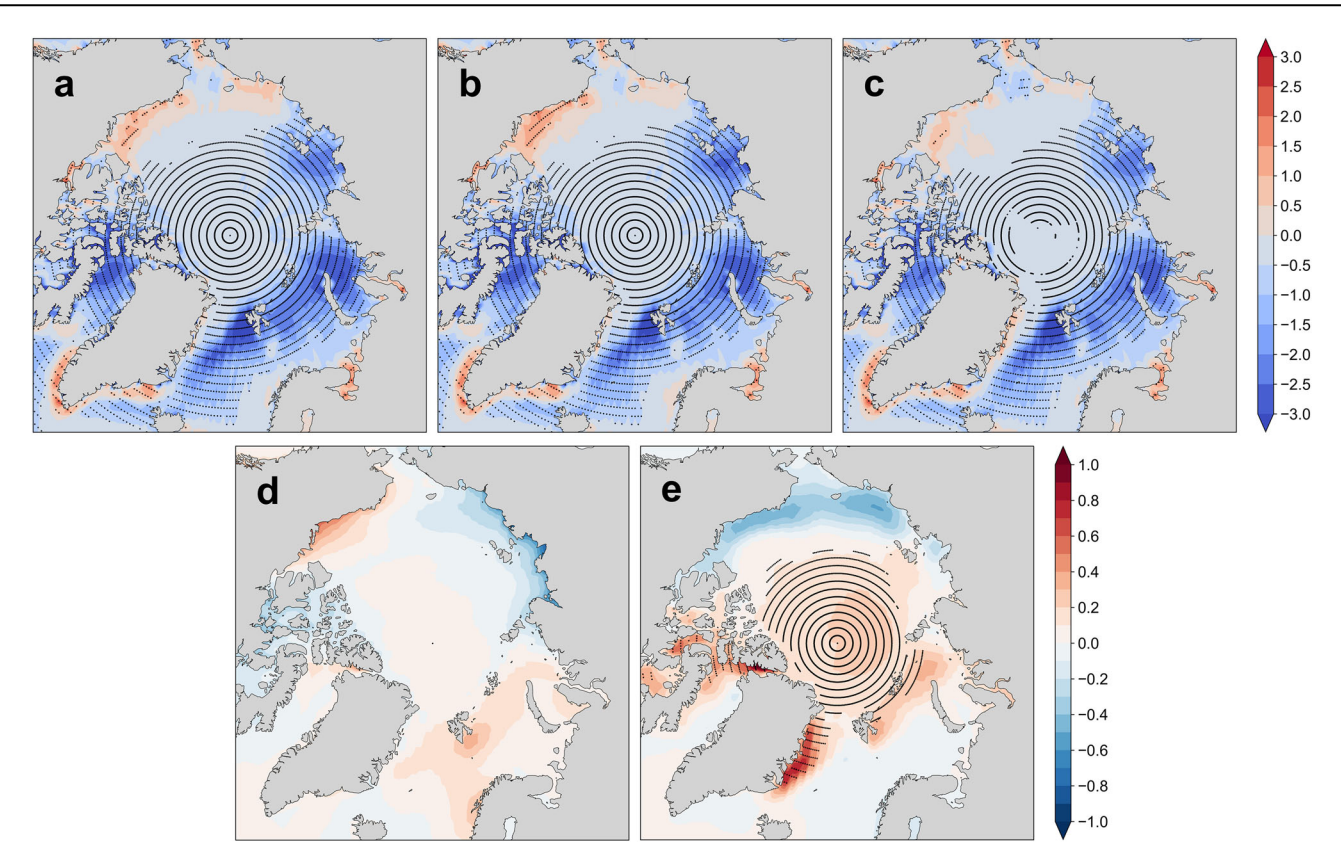


Fig. 8 | Differences in the 20-year averaged surface air temperature (SAT) for August during the hindcast period 2004–2023 (°C). a Control experiment minus observations, (b) SIC-only experiment minus observations, (c) SIC-SIT experiment

minus observations, (d) SIC-only experiment minus Control experiment, (e) SIC-SIT experiment minus Control experiment. Dotted areas indicate statistical significance based on a two-tailed Student's t-test at the 95% confidence level.

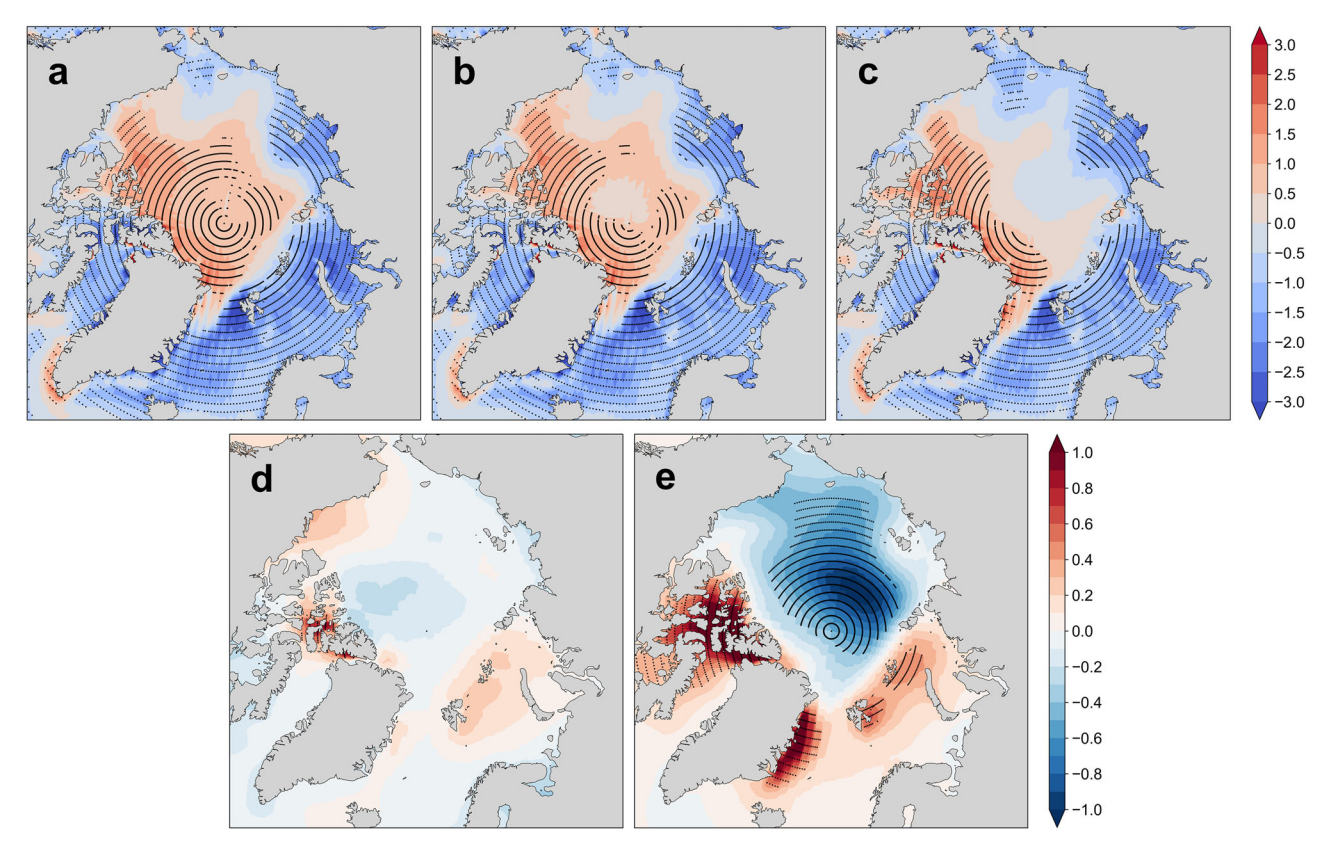


Fig. 9 | Differences in the 20-year averaged SAT for September during the hindcast period 2004–2023 (°C). a Control experiment minus observations, b SIC-only experiment minus observations, c SIC-SIT experiment minus observations,

d SIC-only experiment minus Control experiment, **e** SIC-SIT experiment minus Control experiment. Dotted areas indicate statistical significance based on a two-tailed Student's t test at the 95% confidence level.

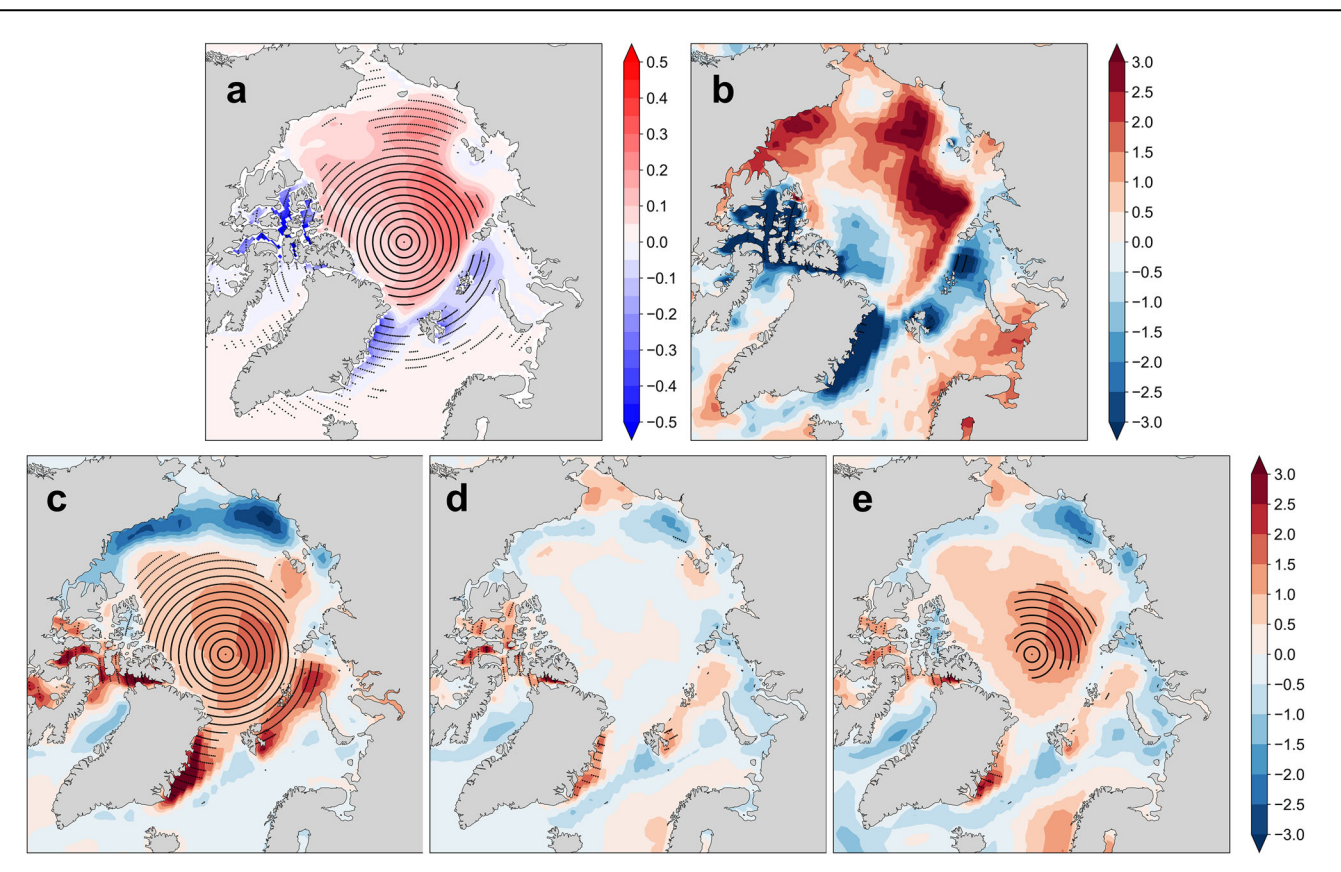


Fig. 10 | Differences in the 20-year averaged SIC and energy fluxes for the hindcast period 2004–2023 in August between the SIC-SIT and Control experiments. Differences in (a) SIC, (b) net shortwave radiation flux (W/m^2) . (c)

Outgoing longwave radiation flux (W/m^2) . (d) Sensible heat flux (W/m^2) . (e) Latent heat flux (W/m^2) . Dotted areas indicate statistical significance based on a two-tailed Student's t-test at the 95% confidence level. All fluxes are positive upwards.

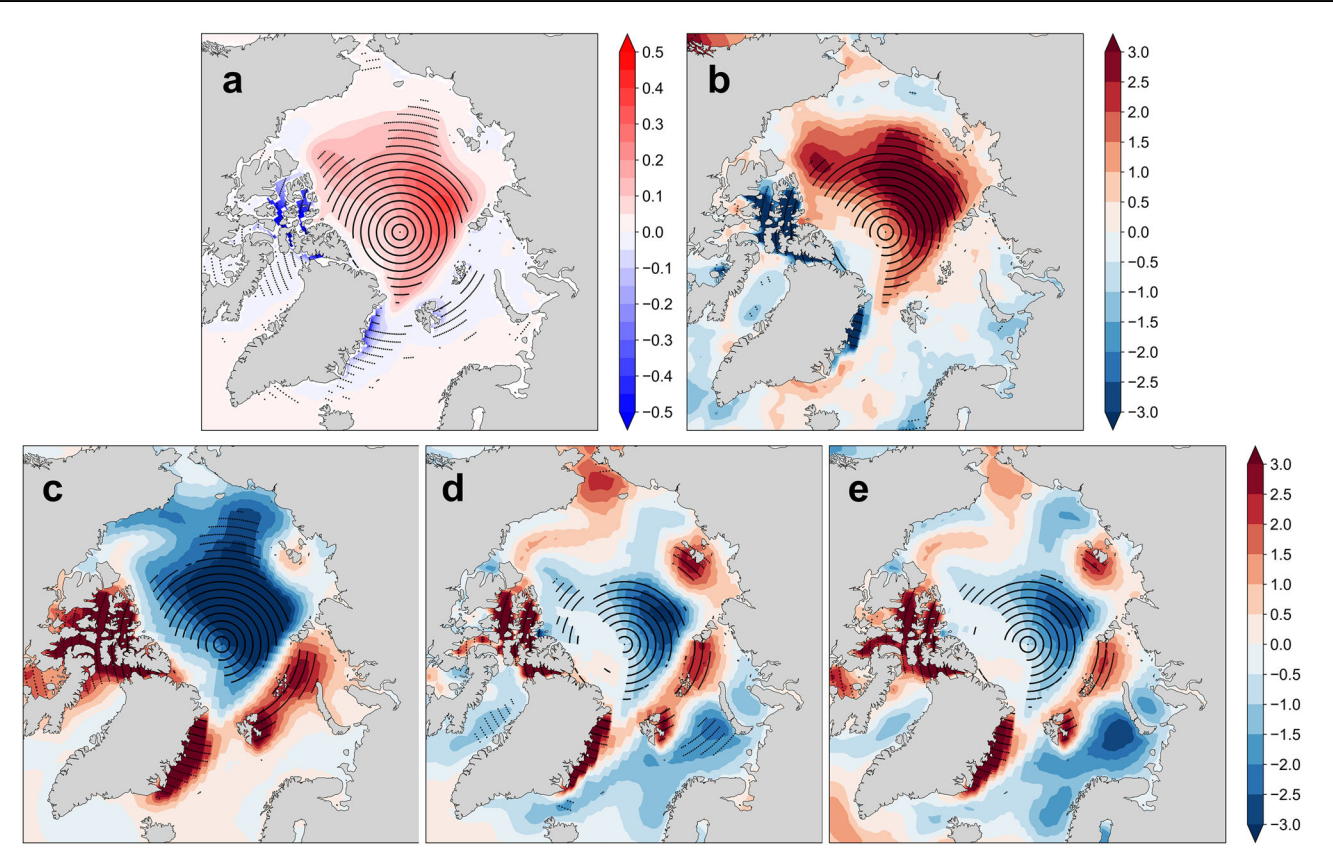


Fig. 11 | Differences in the 20-year averaged SIC and energy fluxes for the hindcast period 2004–2023 in September between the SIC-SIT and Control experiments. Differences in a SIC, b net shortwave radiation flux (W/m^2) .

c Outgoing longwave radiation flux (W/m²). d Sensible heat flux (W/m²). e Latent heat flux (W/m²). Dotted areas indicate statistical significance based on a two-tailed Student's t test at the 95% confidence level. All fluxes are positive upwards.

temperature in the central Arctic even with greater ice coverage, amplifying upward surface longwave radiation and further warming the lower atmosphere. Additionally, observational data analysis reveals a significant positive correlation between year-to-year variations of summer SIC and SAT in the central ice-covered regions (Fig. S2), reinforcing the connection between sea ice changes and surface temperature variations discussed above.

In the September prediction, the overestimated SIC over the East Greenland Sea and the Canadian Archipelago in the Control experiment is similarly reduced in the SIC-SIT experiment, along with a reduction in the cold biases of SAT (Fig. 9a). Similar to August, the open waters continue to absorb solar radiation, increasing upward longwave radiation and sensible heat flux, which further warms the lower atmosphere (Fig. 9b-d). In the northern Barents-Kara Seas, despite minimal changes in SIC and net downward shortwave radiation, the original cold biases of SAT are evidently reduced. This improvement is largely attributed to the strong thermal memory of the sea surface temperature^{58,59}, allowing the higher surface temperatures from August to persist into September, which continue to enhance upward longwave radiation and sensible heat flux, thereby improving the SAT prediction. As solar radiation decreases in September and the melting of sea ice slows, the thermodynamic properties of the central Arctic sea ice gradually align with those of the marginal seas. The underestimated SIC in the Control experiment corresponds to the warm biases of SAT. After assimilation, the reduction in the original warm biases of SAT is primarily due to increased SIC, which enhances albedo and reduces absorbed solar radiation, leading to lower surface temperature. The cooler surface temperature decreases upward longwave radiation and sensible heat flux, further cooling the lower atmosphere.

In summary, optimized sea ice initial conditions improve the surface energy budget predictions, thereby enhancing the subseasonal prediction of SAT. Notably, the impact of sea ice initial condition lasts up to two months, challenging the traditional view that initial conditions affect only short-term forecasts.

Discussion

Accurate subseasonal prediction in the Arctic remains challenging in the current operational systems, especially during the melting season (August–September). Utilizing the LESTKF method within the PDAF framework, this study confirms that sea ice assimilation effectively improves initial conditions and enhances subseasonal predictions in the Arctic with lead times of up to two months. While SIC assimilation alone mainly benefits one-month lead sea ice predictions, incorporating both SIC and SIT produces substantial improvements for both one- and two-month leads. SIC assimilation alone has minimal impact on SAT predictions, whereas adding SIT assimilation significantly improves SAT forecasts for up to two months. This improvement is primarily due to more realistic surface budget predictions, challenging the conventional notion that initial conditions affect only short-term forecasts.

Although sea ice initialization reduces biases in SAT predictions with lead times of up to two months, the improvements remain modest relative to the original errors. While sea ice predictions are substantially improved (by approximately 46% to 96%), the more limited gains in SAT prediction skill suggest that current models may not fully capture the complex feedback between the ice surface and atmosphere⁶⁰. This limitation underscores the potential for further improvement in the sea ice–atmosphere coupling, which could enhance subseasonal predictions both in the Arctic and the broader atmospheric system.

This study highlights the critical role of summer SIT assimilation in enhancing subseasonal predictions of both sea ice and atmospheric conditions, reinforcing SIT as an indispensable source of predictability for subseasonal dynamical forecasts. Strengthening SIT observational capabilities during summer is essential for providing more accurate and stable sea ice initial conditions. Given the challenges in obtaining comprehensive SIT data across the Arctic, a promising approach is to conduct sensitivity experiments in different regions to assess the influence of ice thickness on SIC changes. A similar strategy has been proposed for predicting sea ice volume

(SIV) anomalies, where statistical models identified a small number of optimal locations that account for most of the interannual SIV variability⁶¹. Such experiments could guide targeted efforts to deploy additional SIT observation points in areas with high sensitivity, ultimately providing more reliable SIT initial conditions for subseasonal prediction systems.

Methods

The fully-coupled dynamical model FGOALS-f2

The operational subseasonal prediction system FGOALS-f2 utilized in this study is developed by the State Key Laboratory of Numerical Modeling for Atmospheric Sciences and Geophysical Fluid Dynamics (LASG) at the Institute of Atmospheric Physics (IAP), which is part of the Chinese Academy of Sciences (CAS). FGOALS-f2 is a fully coupled model that encompasses four components: atmosphere, ocean, land, and sea ice. The atmospheric component is version 2 of the Finite-volume Atmospheric Model (FAMIL2)⁶², which uses a finite-volume method⁶³ that is discretized on a cube-sphere grid system⁶⁴. It has a standard horizontal resolution of C96, which means 96 × 96 grid points in each tile of the cube sphere, roughly equivalent to 1-degree resolution. Vertically, it features 32 hybrid sigmapressure levels, with the uppermost level situated at 1 hPa. The land surface component used in FGOALS-f2 is version 4 of the Community Land Model (CLM4.0)⁶⁵, featuring a horizontal resolution nearly at 1-degree resolution. The oceanic component is Parallel Ocean Program version 2 (POP2)66, which utilizes a displaced-pole grid with the North Pole shifted to Greenland. This grid has a resolution of gx1v6, approximately equivalent to a 1-degree horizontal resolution, and includes 60 vertical layers. The sea ice component is the Los Alamos Sea Ice Model version 4.0 (CICE4)⁶⁷, sharing the exact horizontal resolution as the ocean model. These four components are coupled via the coupler version 7 in the Community Earth System Model $(CESM)^{68}$.

The FGOALS-f2 model adopts a Newtonian nudging method with time-varying treatment⁶⁹ to initialize the atmospheric and oceanic conditions. The atmospheric component of the model uses 3-dimensional initial conditions, including temperature, wind, humidity, and geopotential height, obtained from the China Meteorological Administration Global Reanalysis $(CRA-40)^{70}$. The relaxation time scale used in this process is 6 h. In the oceanic component, the Optimal Interpolation Sea Surface Temperature (OISST)⁷¹ from the National Oceanic and Atmospheric Administration (NOAA) is used as the observation to relax the first layer of oceanic temperature, with a 1-day relaxation time scale. No sea ice observations are directly assimilated in the original version. Sea ice concentration, thickness, and horizontal displacement are determined by the thermodynamic and dynamic balance between the overlying atmosphere and underlying ocean water. The model utilizes the time-lagged method to generate ensemble members. For a more detailed explanation of the initialization scheme for FGOALS-f2, please refer to previous studies^{72,73}.

Data assimilation scheme for sea ice

In this study, we use the LESTKF method provided by PDAF, an open-source software for ensemble data assimilation, to incorporate sea ice assimilation into the fully-coupled dynamical model FGOALS-f2. The LESTKF is an advanced data assimilation technique derived from the Ensemble Kalman Filter (EnKF) that incorporates localization and operates within an error subspace. Building on the principles of the Error Subspace Transform Kalman Filter (ESTKF), it updates ensemble members by performing linear transformations within the error subspace generated by ensemble samples⁷⁴. LESTKF introduces localization to selectively limit the influence of observations to relevant neighboring areas, minimizing sampling errors and enhancing the capture of local features. This approach reduces computational complexity by avoiding the direct calculation of high-dimensional error covariance matrices, making it well-suited for high-dimensional nonlinear systems⁵². The LESTKF method has been shown to be effective in sea ice assimilation⁷⁵⁻⁷⁷.

The initialization procedure consists of two main steps: ensemble generation and assimilation. The assimilation window is set from July 18th

to August 1st for each year. To generate ensembles, 7-day simulations are conducted from July 15th to July 21st for each of the past 20 years (2004–2023), during which the daily model state vectors of SIC and SIT are saved. These daily fields are concatenated to construct a state matrix that characterizes the spatiotemporal variability of SIC and SIT during the preassimilation period. Leading empirical orthogonal function (EOF) modes of this matrix are then extracted to reduce dimensionality while retaining dominant variability structures. Sixteen ensemble perturbations are generated using second-order exact sampling⁷⁸ applied in the EOF space and superimposed onto the mean state of model trajectories, thereby forming the initial ensemble spread. Once the ensembles are generated, the LESTKF is applied in analysis cycles to assimilate observed SIC and SIT fields along with their observational uncertainties. The same procedure is applied when assimilating SIC alone. Here, the observational uncertainty is set to 15% for SIC and 0.75 m for SIT. The overall assimilation strategy, including ensemble size and observational uncertainty settings, draws upon previous studies^{36,75–77}. Further details are provided in the Supplementary Information.

Sea ice data for assimilation

The daily SIC data are obtained from the Near-Real-Time NOAA/NSIDC Climate Data Record (CDR) of Passive Microwave Sea Ice Concentration⁷⁹, which integrates estimates derived from the NASA Team and Bootstrap algorithms. The data are provided on the NSIDC polar stereographic grid with a spatial resolution of 25 km. Monthly SIC is calculated by averaging the daily values over each month.

We use thickness data from the Pan-Arctic Ice Ocean Modeling and Assimilation System (PIOMAS)⁸⁰ for assimilation, considering its long temporal coverage, daily resolution, and complete Arctic-wide spatial coverage. Previous studies have demonstrated that the PIOMAS SIT is in reasonable agreement with observations^{80,81} and is suitable for sea ice assimilation^{82–84}. We also tested the assimilation of CryoSat-2 SIT data over the 2011–2020 period³⁴. While CryoSat-2 assimilation improves prediction skill during the first two weeks, the improvement rapidly declines afterward (Fig. S3), likely due to the thinner initial SIT increasing sensitivity to melting (Fig. S4). This suggests that Arctic sea ice prediction is highly sensitive to the choice of SIT data for initialization, underscoring the importance of improving summertime SIT accuracy for better prediction skill during the melting season.

Atmospheric and oceanic data for nudging

In addition to sea ice assimilation, this study also applies atmospheric and oceanic nudging to improve the initial conditions. The atmospheric data used for nudging come from the CRA-40 daily reanalysis dataset 70 provided by the China Meteorological Administration, with a resolution of $0.5^{\circ} \times 0.5^{\circ}$. The variables include temperature, wind, humidity, and geopotential height. The SST data used for nudging is obtained from the NOAA OISST daily dataset 71 , with a resolution of $0.25^{\circ} \times 0.25^{\circ}$.

Persistence calculation

Our calculation of persistence follows the definition provided by Zampieri et al. (2018)²⁰. Persistence is computed based on the initial SIC. Taking 2023 as an example, the daily prediction skill is assessed using observed SIC on each target day as the reference. The persistence forecast ensemble is constructed from SIC fields on August 1st during 2004–2023. To match the size of the model ensemble, 16 samples are randomly selected from the 20 years using a bootstrap method, repeated 1000 times to obtain an averaged benchmark. This approach provides a persistence benchmark consistent with the ensemble size of the model prediction, enabling a robust comparison of prediction skill.

Evaluation methods

Daily SIC data from the NOAA/NSIDC CDR of Passive Microwave Sea Ice Concentration⁷⁹ are used to evaluate SIC prediction skill. The observed SIE, defined as the total area of grid boxes with at least 15% SIC, is calculated

from this dataset. Monthly SIC is calculated by averaging the daily values over each month. For atmospheric verification, the ERA5 monthly reanalysis dataset provided by the European Center for Medium-Range Weather Forecasts (ECMWF) is used 85 . The dataset has a spatial resolution of $0.25^{\circ} \times 0.25^{\circ}$ and includes variables such as 2-meter temperature, net shortwave radiation flux, outgoing longwave radiation flux, sensible heat flux, and latent heat flux.

To comprehensively assess the performance of the data assimilation, we evaluate the spatial and temporal accuracy of SIC and SIE using several metrics. Specifically, the MAE of the SIC spatial distribution is calculated to quantify the average spatial discrepancy between predicted and observed SIC. The ACC and RMSE of SIE anomalies are used to assess the model's skill in capturing both the sign and amplitude of sea ice anomalies. Given the long-term trend dominates the total variability, we remove the linear trend from the SIE anomalies to focus on interannual fluctuations. The linear trend is calculated using the least squares method. The statistical significance of the ACC and RMSE is assessed using the Monte Carlo test, whereby the ACC and RMSE are computed after randomizing the predictions. This procedure is repeated 1000 times, and the significance is defined as the fraction of times the actual prediction ACC (RMSE) is greater (less) than ACC (RMSE) achieved with the randomized set. The significance of differences is tested using a two-tailed Student's t-test. The BS is calculated to evaluate the reliability of the probabilistic predictions regarding the presence or absence of sea ice, with a focus on capturing ice edge position and occurrence probability.

The MAE of SIC spatial distribution is calculated as:

$$MAE = \frac{1}{N} \sum_{i=1}^{N} \left| SIC_{pre,i} - SIC_{obs,i} \right|$$

where $SIC_{pre,i}$ and $SIC_{obs,i}$ represent the predicted and observed SIC values for grid cell i, respectively. Here, N represents the total number of grid cells where the difference between predicted and observed values is statistically significant at the 95% level.

The ACC for SIE anomalies is calculated as:

$$ACC = \frac{\sum_{t=1}^{T} \left(SIE_{pre,t} - \overline{SIE}_{pre}\right) \left(SIE_{obs,t} - \overline{SIE}_{obs}\right)}{\sqrt{\sum_{t=1}^{T} \left(SIE_{pre,t} - \overline{SIE}_{pre}\right)^{2}} \times \sqrt{\sum_{t=1}^{T} \left(SIE_{obs,t} - \overline{SIE}_{obs}\right)^{2}}}$$

where $SIE_{pre,t}$, $SIE_{obs,t}$ represent the predicted and observed SIE anomalies at time t, and T is the total number of years. The time averages for prediction and observation, \overline{SIE}_{pre} and \overline{SIE}_{obs} , are calculated by $\frac{1}{T}\sum_{t=1}^{T}SIE_{pre,t}$ and $\frac{1}{T}\sum_{t=1}^{T}SIE_{obs,t}$, respectively.

The RMSE for SIE anomalies is calculated as:

$$\mathit{RMSE} = \sqrt{\frac{1}{T} \sum_{t=1}^{T} \left(\mathit{SIE}_{\mathit{pre},t} - \mathit{SIE}_{\mathit{obs},t}\right)^2}$$

where $SIE_{pre,t}$, $SIE_{obs,t}$ represent the predicted and observed SIE anomalies at time t, and T is the total number of years.

The BS scores for SIC distribution is calculated as:

$$BS = \frac{1}{N} \sum_{i=1}^{N} (f_i - o_i)^2$$

where f_i is the predicted probability of sea ice presence in grid cell i, o_i is the observed binary outcome (1 for $SIC \ge 15\%$ and 0 otherwise), and N is the total number of grid cells across all Arctic seas (similar to Wayand et al., 2019)²¹.

Data availability

Daily SIC data used for assimilation and validation are available from the Near-Real-Time NOAA/NSIDC CDR of Passive Microwave Sea Ice Concentration (https://nsidc.org/data/g02202/versions/4). Daily PIOMAS SIT data can be accessed at https://psc.apl.uw.edu/research/projects/arctic-sea-ice-volume-anomaly/data. Weekly Cryosat-2 SIT data are available from the British Antarctic Survy (https://data.bas.ac.uk/full-record.php?id=GB/NERC/BAS/PDC/01613). Atmospheric variables used for assimilation, including temperature, wind, humidity, and geopotential height, are available from the CRA-40 daily reanalysis dataset (https://data.cma.cn/analysis/cra40). SST data used for assimilation are available from the NOAA OISST daily dataset (https://www.ncei.noaa.gov/products/optimum-interpolation-sst). ERA5 monthly reanalysis dataset for atmospheric validation is obtained from ECMWF (https://cds.climate.copernicus.eu/datasets/reanalysis-era5-single-levels-monthly-means?tab=download).

Code availability

All codes for the analysis of this paper are available from the corresponding author upon reasonable request.

Received: 20 December 2024; Accepted: 15 April 2025; Published online: 06 June 2025

References

- Stroeve, J. & Notz, D. Changing state of Arctic sea ice across all seasons. *Environ. Res. Lett.* 13, 103001 (2018).
- Yu, Q., Wu, B. & Zhang, W. The atmospheric connection between the Arctic and Eurasia is underestimated in simulations with prescribed sea ice. Commun. Earth Environ. 5, 435 (2024).
- Stroeve, J., Hamilton, L. C., Bitz, C. M. & Blanchard-Wrigglesworth, E. Predicting September sea ice: Ensemble skill of the SEARCH Sea Ice Outlook 2008-2013. Geophys. Res. Lett. 41, 2411–2418 (2014).
- Blanchard-Wrigglesworth, E. et al. Forecast skill of the Arctic Sea Ice Outlook 2008–2022. Geophys. Res. Lett. 50, e2022GL102531 (2023).
- Smith, L. C. & Stephenson, S. R. New Trans-Arctic shipping routes navigable by midcentury. *Proc. Natl. Acad. Sci. USA* 110, E1191–E1195 (2013).
- Melia, N., Haines, K. & Hawkins, E. Sea ice decline and 21st century trans-Arctic shipping routes. *Geophys. Res. Lett.* 43, 9720–9728 (2016).
- Min, C. et al. The emerging arctic shipping corridors. Geophys. Res. Lett. 49, e2022GL099157 (2022).
- Niittynen, P., Heikkinen, R. K. & Luoto, M. Snow cover is a neglected driver of Arctic biodiversity loss. Nat. Clim. Chang. 8, 997–1001 (2018).
- Avango, D., Nilsson, A. E. & Roberts, P. Assessing Arctic futures: voices, resources and governance. *Polar J.* 3, 431–446 (2013).
- Bergmann, M. et al. Plastic pollution in the Arctic. Nat. Rev. Earth Environ. 3, 323–337 (2022).
- Liu, A. et al. Subseasonal-to-seasonal prediction of Arctic sea ice using a fully coupled dynamical ensemble forecast system. *Atmos. Res.* 295, 107014 (2023).
- Wang, W., Chen, M. & Kumar, A. Seasonal prediction of Arctic sea ice extent from a coupled dynamical forecast system. *Mon. Weather Rev.* 141, 1375–1394 (2013).
- Jung, T. et al. Advancing polar prediction capabilities on daily to seasonal time scales. Bull. Am. Meteorol. Soc. 97, 1631–1647 (2016).
- McGraw, M. C., Blanchard-Wrigglesworth, E., Clancy, R. P. & Bitz, C. M. Understanding the forecast skill of rapid Arctic sea ice loss on subseasonal time scales. *J. Clim.* 35, 1179–1196 (2022).
- Liu, Y., Wang, W. & Kumar, A. Multiweek prediction skill assessment of Arctic sea ice variability in the CFSv2. Weather Forecast 33, 1453–1476 (2018).
- Liu, J. et al. Towards reliable Arctic sea ice prediction using multivariate data assimilation. Sci. Bull. 64, 63–72 (2019).
- Zhang, Y.-F. et al. Assimilation of satellite-retrieved sea ice concentration and prospects for September predictions of Arctic sea ice. J. Clim. 34, 2107–2126 (2021).

- Massonnet, F., Fichefet, T. & Goosse, H. Prospects for improved seasonal Arctic sea ice predictions from multivariate data assimilation. *Ocean Model.* 88, 16–25 (2015).
- Kimmritz, M. et al. Impact of ocean and sea ice initialisation on seasonal prediction skill in the Arctic. J. Adv. Model. Earth Syst. 11, 4147–4166 (2019).
- Zampieri, L., Goessling, H. F. & Jung, T. Bright prospects for Arctic sea ice prediction on subseasonal time scales. *Geophys. Res. Lett.* 45, 9731–9738 (2018).
- Wayand, N. E., Bitz, C. M. & Blanchard-Wrigglesworth, E. A year-round subseasonal-to-seasonal sea ice prediction portal. *Geophys. Res. Lett.* 46, 3298–3307 (2019).
- Blockley, E. W. & Peterson, K. A. Improving Met Office seasonal predictions of Arctic sea ice using assimilation of CryoSat-2 thickness. Cryosphere 12, 3419–3438 (2018).
- Goessling, H. F., Tietsche, S., Day, J. J., Hawkins, E. & Jung, T. Predictability of the Arctic sea ice edge. *Geophys. Res. Lett.* 43, 1642–1650 (2016).
- Tietsche, S., Notz, D., Jungclaus, J. H. & Marotzke, J. Predictability of large interannual Arctic sea-ice anomalies. *Clim. Dyn.* 41, 2511–2526 (2013).
- Blanchard-Wrigglesworth, E., Armour, K. C., Bitz, C. M. & DeWeaver,
 E. Persistence and inherent predictability of Arctic sea ice in a GCM ensemble and observations. J. Clim. 24, 231–250 (2011).
- Blanchard-Wrigglesworth, E., Bitz, C. M. & Holland, M. M. Influence of initial conditions and climate forcing on predicting Arctic sea ice. *Geophys. Res. Lett.* https://doi.org/10.1029/2011GL048807 (2011).
- Day, J. J., Hawkins, E. & Tietsche, S. Will Arctic sea ice thickness initialization improve seasonal forecast skill? *Geophys. Res. Lett.* 41, 7566–7575 (2014).
- Fiedler, E. K. et al. Assimilation of sea ice thickness derived from CryoSat-2 along-track freeboard measurements into the Met Office's Forecast Ocean Assimilation Model (FOAM). Cryosphere 16, 61–85 (2022).
- Mignac, D., Martin, M., Fiedler, E., Blockley, E. & Fournier, N. Improving the Met Office's Forecast Ocean Assimilation Model (FOAM) with the assimilation of satellite-derived sea-ice thickness data from CryoSat-2 and SMOS in the Arctic. Q. J. R. Meteorol. Soc. 148, 1144–1167 (2022).
- Williams, N. et al. The effects of assimilating a sub-grid-scale sea ice thickness distribution in a new Arctic sea ice data assimilation system. Cryosphere 17, 2509–2532 (2023).
- Bonan, D. B., Bushuk, M. & Winton, M. A spring barrier for regional predictions of summer Arctic sea ice. *Geophys. Res. Lett.* 46, 5937–5947 (2019).
- 32. Bushuk, M., Winton, M., Bonan, D. B., Blanchard-Wrigglesworth, E. & Delworth, T. L. A mechanism for the Arctic sea ice spring predictability barrier. *Geophys. Res. Lett.* **47**, e2020GL088335 (2020).
- 33. Zeng, J. et al. Reducing the spring barrier in predicting summer Arctic sea ice concentration. *Geophys. Res. Lett.* **50**, e2022GL102115 (2023).
- Landy, J. C. et al. A year-round satellite sea-ice thickness record from CryoSat-2. Nature 609, 517–522 (2022).
- Zhang, Y.-F. et al. Improvements in September Arctic sea ice predictions via assimilation of summer CryoSat-2 sea ice thickness observations. *Geophys. Res. Lett.* 50, e2023GL105672 (2023).
- Song, R., Mu, L., Loza, S. N., Kauker, F. & Chen, X. Assimilating summer sea-ice thickness observations improves Arctic sea-ice forecast. *Geophys. Res. Lett.* 51, e2024GL110405 (2024).
- Vitart, F. et al. The Subseasonal to Seasonal (S2S) Prediction Project database. Bull. Am. Meteorol. Soc. 98, 163–173 (2017).
- White, C. J. et al. Potential applications of subseasonal-to-seasonal (S2S) predictions. *Meteorol. Appl.* 24, 315–325 (2017).
- Yang, J. et al. Late-July barrier for subseasonal forecast of summer daily maximum temperature over Yangtze River Basin. *Geophys. Res.* Lett. 45, 610–12,615 (2018).

- Liang, P. & Lin, H. Sub-seasonal prediction over East Asia during boreal summer using the ECCC monthly forecasting system. *Clim. Dvn.* 50, 1007–1022 (2017).
- Weyn, J. A., Durran, D. R., Caruana, R. & Cresswell-Clay, N. Subseasonal forecasting with a large ensemble of deep-learning weather prediction models. *J. Adv. Model. Earth Syst.* 13, e2021MS002502 (2021).
- Buizza, R. & Leutbecher, M. The forecast skill horizon. Q. J. R. Meteorol. Soc. 141, 3366–3382 (2015).
- Acosta Navarro, J. C. et al. Link between autumnal Arctic sea ice and Northern Hemisphere winter forecast skill. *Geophys. Res. Lett.* 47, e2019GL086753 (2020).
- Cohen, J. et al. Recent Arctic amplification and extreme mid-latitude weather. *Nat. Geosci.* 7, 627–637 (2014).
- Liu, J., Curry, J. A., Wang, H., Song, M. & Horton, R. M. Impact of declining Arctic sea ice on winter snowfall. *Proc. Natl Acad. Sci. USA* 109, 4074–4079 (2012).
- Wu, B., Yang, K. & Francis, J. A. A cold event in Asia during January–February 2012 and its possible association with Arctic sea ice loss. J. Clim. 30, 7971–7990 (2017).
- Dai, G. et al. The influence of Arctic sea ice concentration perturbations on subseasonal predictions of North Atlantic Oscillation events. Adv. Atmos. Sci. 40, 2242–2261 (2023).
- Ma, X. et al. Influence of Arctic sea ice concentration on extendedrange prediction of strong and long-lasting Ural blocking events in winter. J. Geophys. Res. Atmos. 127, e2021JD036282 (2022).
- Li, C. et al. Influence of Arctic sea-ice concentration on extendedrange forecasting of cold events in East Asia. Adv. Atmos. Sci. 40, 2224–2241 (2023).
- Li, J. et al. Dynamical seasonal prediction of tropical cyclone activity using the FGOALS-f2 ensemble prediction system. Weather Forecast 36, 1759–1778 (2021).
- 51. Bao, Q. & Li, J. Progress in climate modeling of precipitation over the Tibetan Plateau. *Natl Sci. Rev.* **7**, 486–487 (2020).
- Nerger, L., Janjić, T., Schröter, J. & Hiller, W. A regulated localization scheme for ensemble-based Kalman filters. Q. J. R. Meteorol. Soc. 138, 802–812 (2011).
- Nerger, L. & Hiller, W. Software for ensemble-based data assimilation systems—Implementation strategies and scalability. *Comput.* Geosci. 55, 110–118 (2013).
- Brier, G. W. Verification of forecasts expressed in terms of probability. *Mon. Weather Rev.* 78, 1–3 (1950).
- 55. Liu, Y., Bogaardt, L., Attema, J. & Hazeleger, W. Extended range Arctic sea ice forecast with convolutional long-short term memory networks. *Mon. Weather Rev.* **149**, 1673–1693 (2021).
- Liu, J., Curry, J. A. & Hu, Y. Recent Arctic sea ice variability: Connections to the Arctic Oscillation and the ENSO. *Geophys. Res. Lett.* https://doi.org/10.1029/2004GL019858 (2004).
- Davidson, E. A. & Janssens, I. A. Temperature sensitivity of soil carbon decomposition and feedbacks to climate change. *Nature* 440, 165–173 (2006).
- Deser, C., Alexander, M. A., Xie, S. P. & Phillips, A. S. Sea surface temperature variability: Patterns and mechanisms. *Annu. Rev. Mar.* Sci. 2, 115–143 (2010).
- Deser, C., Alexander, M. A. & Timlin, M. S. Understanding the persistence of sea surface temperature anomalies in midlatitudes. *J. Clim.* 16, 57–72 (2003).
- Guemas, V. et al. Impact of sea ice initialization on sea ice and atmosphere prediction skill on seasonal timescales. *Geophys. Res. Lett.* 43, 3889–3896 (2016).
- Ponsoni, L. et al. Statistical predictability of the Arctic sea ice volume anomaly: identifying predictors and optimal sampling locations. Cryosphere 14, 2409–2428 (2020).

- Li, J. et al. Evaluation of FAMIL2 in simulating the climatology and seasonal-to-interannual variability of tropical cyclone characteristics. *J. Adv. Model. Earth Syst.* 11, 1117–1136 (2019).
- Lin, S.-J. A "vertically Lagrangian" finite-volume dynamical core for global models. *Mon. Weather Rev.* 132, 2293–2307 (2004).
- Putman, W. M. & Lin, S.-J. Finite-volume transport on various cubedsphere grids. J. Comput. Phys. 227, 55–78 (2007).
- 65. Lawrence, D. M. et al. Parameterization improvements and functional and structural advances in version 4 of the Community Land Model. *J. Adv. Model. Earth Syst.* **3**, n/a–n/a (2011).
- Kerbyson, D. J. & Jones, P. W. A performance model of the parallel ocean program. *Int. J. High. Perform. Comput. Appl.* 19, 261–276 (2005).
- Hunke, E. C. & Lipscomb, W. H. CICE: The Los Alamos sea ice model, documentation and software user's manual version 4.1. Tech. Rep. LA-CC-06-012 (2010).
- Craig, A. P., Vertenstein, M. & Jacob, R. A new flexible coupler for earth system modeling developed for CCSM4 and CESM1. *Int. J. High. Perform. Comput. Appl.* 26, 31–42 (2011).
- Jeuken, A. B. M., Siegmund, P. C., Heijboer, L. C., Feichter, J. & Bengtsson, L. On the potential of assimilating meteorological analyses in a global climate model for the purpose of model validation. *J. Geophys. Res. Atmos.* 101, 16939–16950 (1996).
- Liu, Z. et al. CRA-40/Atmosphere—The first-generation Chinese atmospheric reanalysis (1979–2018): System description and performance evaluation. J. Meteorol. Res. 37, 1–19 (2023).
- Huang, B. et al. Improvements of the daily optimum interpolation sea surface temperature (DOISST) version 2.1. *J. Clim.* 34, 2923–2939 (2021).
- Zeng, L. et al. Impacts of humidity initialization on MJO prediction: A study in an operational sub-seasonal to seasonal system. *Atmos. Res.* 294, 106946 (2023).
- Liu, Y. et al. Dynamical Madden–Julian Oscillation forecasts using an ensemble subseasonal-to-seasonal forecast system of the IAP-CAS model. *Geosci. Model Dev.* 17, 6249–6275 (2024).
- Nerger, L., Janjić, T., Schröter, J. & Hiller, W. A unification of ensemble square root Kalman filters. *Mon. Weather Rev.* 140, 2335–2345 (2012).
- Yang, C. Y., Liu, J. & Xu, S. Seasonal Arctic sea ice prediction using a newly developed fully coupled regional model with the assimilation of satellite sea ice observations. *J. Adv. Model. Earth Syst.* 12, e2019MS001938 (2020).
- Chen, Z., Liu, J., Song, M., Yang, Q. & Xu, S. Impacts of assimilating satellite sea ice concentration and thickness on Arctic sea ice prediction in the NCEP climate forecast system. *J. Clim.* 30, 8429–8446 (2017).
- Mu, L. et al. Toward a data assimilation system for seamless sea ice prediction based on the AWI climate model. *J. Adv. Model. Earth Syst.* 12, e2019MS001937 (2020).
- Pham, D. T. Stochastic methods for sequential data assimilation in strongly nonlinear systems. *Mon. Weather Rev.* 129, 1194–1207 (2001).
- Meier, W. N., Fetterer, F., Windnagel, A. K. & Stewart, S. NOAA/NSIDC climate data record of passive microwave sea ice concentration, version 4. (2021).
- Zhang, J. & Rothrock, D. A. Modeling global sea ice with a thickness and enthalpy distribution model in generalized curvilinear coordinates. *Mon. Weather Rev.* 131, 845–861 (2003).
- Schweiger, A. et al. Uncertainty in modeled Arctic sea ice volume. J. Geophys. Res. Oceans https://doi.org/10.1029/2011JC007084 (2011).
- Collow, T. W., Wang, W., Kumar, A. & Zhang, J. Improving Arctic sea ice prediction using PIOMAS initial sea ice thickness in a coupled ocean–atmosphere model. *Mon. Weather Rev.* 143, 4618–4630 (2015).

- 83. Zhang, J., Lindsay, R., Steele, M. & Schweiger, A. What drove the dramatic retreat of Arctic sea ice during summer 2007? *Geophys. Res. Lett.* https://doi.org/10.1029/2008GL034005 (2008).
- Schutz, B. E., Zwally, H. J., Shuman, C. A., Hancock, D. & DiMarzio, J. P. Overview of the ICESat mission. *Geophys. Res. Lett.* https://doi. org/10.1029/2005GL024009 (2005).
- Hersbach, H. et al. The ERA5 global reanalysis. Q. J. R. Meteorol. Soc. 146, 1999–2049 (2020).

Acknowledgements

Jing Yang was supported by funding from the National Key R&D Program of China (Project No. 2024YFC3013100), the National Natural Science Foundation of China (Project No. 42475022), and the National Natural Science Foundation of China (Project No. 42261144671). Menggian Lu was supported by the General Research Fund (Project No. 16300424). Seong-Joong Kim was supported by the KOPRI project (Project No. PE25010). Jiping Liu was supported by the Southern Marine Science and Engineering Guangdong Laboratory (Zhuhai) (SML2024SP023). This work was supported by the Seamless Prediction and Services for Sustainable Natural and Built Environments (SEPRESS) Program (2025-2032). The authors acknowledge the support from the Otto Poon Centre for Climate Resilience and Sustainability at HKUST. Data processing and storage were supported by the National Key Scientific and Technological Infrastructure project "Earth System Numerical Simulation Facility" (EarthLab). The authors are grateful for the highperformance computing support from the Center for Geodata and Analysis, Faculty of Geographical Science, Beijing Normal University.

Author contributions

Conceptualization: A.L., J.Y. Methodology: A.L., J.Y. Writing—original draft: A.L., J.Y. Visualization: A.L. Supervision: A.L., J.Y., Q.B. Writing—review & editing: A.L., J.Y., Q.B., F.V., J.L., X.L., M.L., S.-J.K., D.G., Z.T., H.L.

Competing interests

The authors declare no competing interests.

Additional information

Supplementary information The online version contains supplementary material available at https://doi.org/10.1038/s41612-025-01050-8.

Correspondence and requests for materials should be addressed to Jing Yang.

Reprints and permissions information is available at http://www.nature.com/reprints

Publisher's note Springer Nature remains neutral with regard to jurisdictional claims in published maps and institutional affiliations.

Open Access This article is licensed under a Creative Commons Attribution-NonCommercial-NoDerivatives 4.0 International License, which permits any non-commercial use, sharing, distribution and reproduction in any medium or format, as long as you give appropriate credit to the original author(s) and the source, provide a link to the Creative Commons licence, and indicate if you modified the licensed material. You do not have permission under this licence to share adapted material derived from this article or parts of it. The images or other third party material in this article are included in the article's Creative Commons licence, unless indicated otherwise in a credit line to the material. If material is not included in the article's Creative Commons licence and your intended use is not permitted by statutory regulation or exceeds the permitted use, you will need to obtain permission directly from the copyright holder. To view a copy of this licence, visit http://creativecommons.org/licenses/by-nc-nd/4.0/.

© The Author(s) 2025